ARTICLE

Highly efficient removal of toxic lead ions from aqueous solutions using a new magnetic metal-organic framework nanocomposite

Mohammad Ali Karimi[1] | Hassan Masrouri[2] | Hassan Karami[1] | Saeed Andishgar[1] |
Mehrnaz Alsadat Mirbagheri[1] | Tayebe Pourshamsi[1]

[1]Department of Chemistry, Payame Noor University, Tehran, Iran

[2]Department of Chemistry and Petrochemical Engineering, Standard Research Institute, Karaj, Iran

Correspondence

Mohammad Ali Karimi, Department of Chemistry, Payame Noor University, Tehran 19395-4697, Iran.
Email: ma_karimi43@yahoo.com; m_karimi@pnu.ac.ir

A magnetic metal-organic framework (MOF) nanocomposite was successfully prepared by a new and green strategy through reasonable design. Magnetic MOF of Fe_3O_4-$NHSO_3H$@HKUST-1 nanocomposite use for removal of lead ions as an environmental pollutant. The experimental results indicated that the nano adsorbent of Fe_3O_4-$NHSO_3H$@HKUST-1 can removed lead ions under optimum operational conditions. The dosage of the nanocomposite, pH of the sample solution, and contact time were obtained to be 10 mg, 7.0, and 90 min, respectively, while the initial concentration of Pb(II) ions of 400 mg/L was used. A kinetic study indicated that a pseudo-second-order model agreed well with the experimental data. The isotherm experiments revealed that the Langmuir model attained better fits to the equilibrium data than the Freundlich model. The maximum adsorption capacity of the adsorbent for the removal of lead under the optimum operational conditions of pH 7.0 and temperature 25°C was found to be 384.6 mg/g. The thermodynamic parameters indicate that the adsorption of lead is spontaneous and endothermic. The magnetic MOF nanocomposite could be recovered easily and reused many times without significant loss of its nano-adsorbent activity. The proposed method is simple, eco-friendly, low cost, and efficient in the removal of lead ions from aqueous solutions.

KEYWORDS

hybridized adsorbent, lead ions, magnetic metal-organic framework, nanocomposite, removal

1 | INTRODUCTION

Metal-organic frameworks (MOFs) are a new generation of ordered porous materials. The high porosity, expansion and and contraction of structurally flexible MOFs provides different properties and applications viewpoints including structural characterization, crystal engineering, adsorption-separation applications of gas,[1] as well as the removal of pollutants such as dyes,[2–4] heavy metals,[5,6] toxic compounds,[7,8] and pesticides[9–11] from the environment.

Today, researchers have a tendency to the combination of functional nanoparticles with the MOFs to prepare nano-composites. One of the known HKUST-1 is the $Cu_3(BTC)_2$ MOF (BTC = 1,3,5-benzenetricarboxylate), which is one of the first stable MOFs reported with very high surface area. In this resesrch, HKUST-1 was combined with the magnetite nanoparticles of Fe_3O_4, which are highly appreciated as the core due to their properties such as high coercivity, moderate saturation magnetization, fine mechanical, chemical stability, and low toxicity to the environment.[12] The resulting nanocomposite has exhibit specific functional properties such as easy loading, large pores with wide windows, available coordinative unsaturated sites, high stability of chemical, rapid collection, wide surface area, as well as controllable magnetic characteristics.[13]

The life of all creatures on earth is affected by the serious threat as a result of heavy metals pollution because rapid industrialization and the world population increase. Lead is one of the common contaminants of industrial wastewaters, which results from the manufacture of storage batteries, printing and painting pigments, lead glass, and dyes.[14]

Various methods have been developed for the removal of lead ions from aqueous solutions, including chemical precipitation,[15] ion-exchange,[16] membrane filtration technologies,[17] electroflotation technique,[18] coagulation and flocculation,[19] flotation,[20] preconcentration and extraction,[21,22] and adsorption.[23] Adsorption method is also known as an a practical and economical procedure for lead elimination from wastewater due to easy design and operation of equipment, process reversible, and adsorbent recovery.[24] In many literature have been reported adsorption[25] of heavy metals such as Hg[26] and Cu[27] by magnetic MOF nanocomposites.

The overarching objective of this paper, preparation of magnetic metal-organic framework nanocomposite of Fe_3O_4-NHSO$_3$H@HKUST-1 and study the potentiality of using it as an adsorbent for the removal of lead ions. Then, the effective parameters such as the pH and temperature of the solution, the initial concentration of lead, and the time of contact between the adsorbent and the analyte were investigated. Also, adsorption isotherms, kinetics, and thermodynamic parameters were checked and discussed.

2 | EXPERIMENTAL

2.1 | Reagents and chemicals

The reagents and solvents were bought from Fluka or Merck and consumed without further purification. Ammonia solution (25% m/m), hydrochloric acid (37%), $FeCl_3 \cdot 6H_2O$ (96% m/m), $FeCl_2 \cdot 4H_2O$ (99.9% m/m), 1,3,5-benzenetricarboxylic acid (H$_3$BTC), tetraethoxysilane (TEOS), $Cu(NO_3)_2 \cdot 3H_2O$, 3-aminopropyl-triethoxysilane (99.5%), NH$_4$OH (10%), dimethylformamide, dichloromethane, chlorosulfonic acid, $Pb(NO_3)_2$ (99.5%), and ethanol (96%) were purchased from standard sources. All chemical solutions were prepared using deionized water and by deoxygenating with 99.9% nitrogen for 2 hr. A stock solution of lead at a concentration of 1000 mg/L was prepared by dissolving the appropriate amount of $Pb(NO_3)_2$. The pH of solutions in these experiments was adjusted by HCl and NaOH solutions.

2.2 | Apparatus

A Varian AA 240FS atomic absorption spectrometer (AAS) was employed for the quantification of lead ion concentration. The pH values were monitored by a Metrohm 780 pH meter, supplied with a combined electrode. The magnetic field for magnetic separation was applied by the supermagnet Nd-Fe-B (1.4 T, 10 × 5 × 2 cm). The dispersion of the nanocomposite the solution was performed with ultrasonicator (S60H model, Germany). A Thermo IR-100 infrared spectrometer (Nicolet) was used for recording the Fourier-transform infrared (FTIR) spectra of synthesized nanocomposites. Nanostructures were identified by an X-ray diffractometer (XRD, PW1730 model, Philips, Cu [Kα = 1.54 Å], at the scanning speed of 2°/min and in the range of 2θ = 10°–100°). Transmission electron microscopy (TEM) (JEOL JEM-2010) and field-emission scanning electron microscopy (TEScan—Mira III model FE-SEM) were employed to determine the particle size and surface morphology. The adsorption–desorption isotherms of nitrogen at 77 K were determined using a Micromeritics TriStar II instrument (Model Belsorp mini II, Japan). The magnetization curves of the nanocomposites were measured by a vibrating sample magnetometer (VSM, PPMS-9T).

2.3 | Synthesis of Fe_3O_4-NHSO$_3$H@HKUST-1

Magnetic Fe_3O_4 nanoparticles were synthesized via a chemical co-precipitation method by mixing 5.838 g of $FeCl_3 \cdot 6H_2O$ and 2.147 g of $FeCl_2 \cdot 4H_2O$, as reported previously.[2,28] Second stage of magnetic nanoparticles synthesized by Tetraethoxysilane (TEOS) reaction by a thin layer of silica and iron oxide nanoparticles were covered. In this step, 1.5 g of Fe_3O_4 nanoparticles was dispersed in 10 mL water and 100 mL ethanol by sonication (15 min). Then, 1.4 mL NH$_3$·H$_2$O (10% v/v) was added to the mixture. After 10 min, 3 mL TEOS was added to the reaction solution and stirred mechanically for 12 hr. The harvested particles were separated from the reaction mixture with an external magnetic field, then washed with ethanol for several times, and dried at 50°C under vacuum. 3-Aminopropyltriethoxysilane (APTES) was used as a coupling agent to surface treats the nanoparticles.[28]

Then, 500 mg of APTES-MNPs was dispersed in dry CH_2Cl_2 (3.0 mL) in an ultrasonic bath for 10 min. Subsequently, chlorosulfuric acid (0.6 mL) was added dropwise during 30 min at room temperature. Hydrogen chloride gas evolved from the reaction vessel instantly. The resulting functionalized MNP nanoparticles were extracted by the external magnetic field and washed with dry CH_2Cl_2 for three times.[28]

Then, 30 mg of Fe_3O_4@SiO$_2$-NHSO$_3$H was dispersed in 10 mL ultrapure water using an ultrasonic bath (30 min), and afterwards 0.875 g $Cu(NO_3)_2 \cdot 3H_2O$ (3.62 mmol) was added to the mixture. In another container, 0.42 g of H$_3$BTC (2.0 mmol) was dissolved in ethanol/DMF volume ratio, 10:10 and was added to the mixture. Then, the homogeneous mixture was heated in a 50-mL Teflon-lined autoclave at 120°C for 20 hr. The reaction product (blue crystals) was filtered and washed by DMF and ethanol for several times and dried overnight at 80°C under air atmosphere. The synthetic strategy for Fe_3O_4-NHSO$_3$H@HKUST-1 is presented in Figure 1.
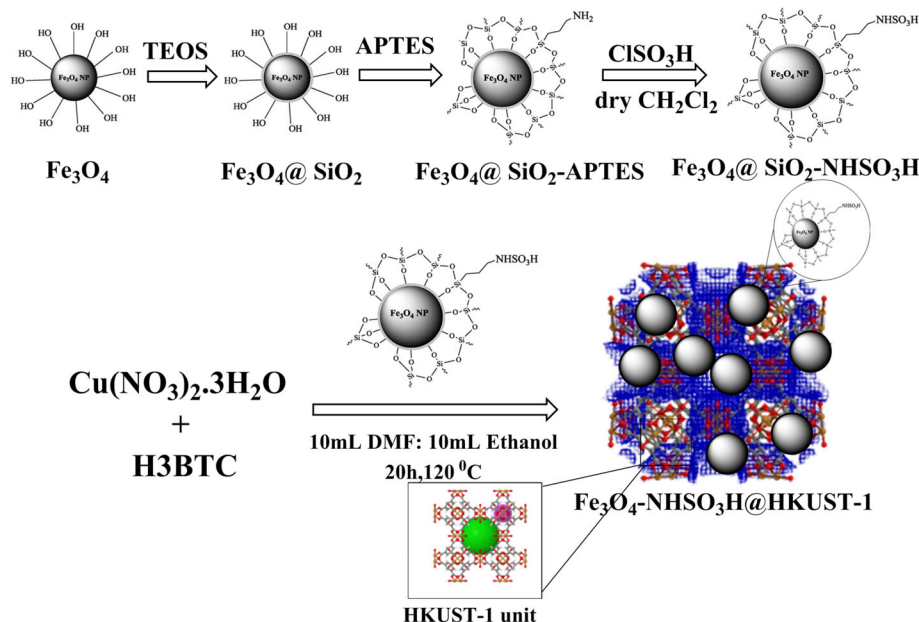
FIGURE 1 Preparation steps of the magnetic metal-organic framework Fe$_3$O$_4$-NHSO$_3$H@HKUST-1 nanocomposite

2.4 | Batch adsorption experiments

To study the effect of the experimental parameters, the batch technique was used. A stock solution (1000 mg/L) of Pb(II) was made (1.60 g of Pb(NO$_3$)$_2$ in 1000 mL of total volume by distilled water).

In each experiment, 50 mL of Pb(II) solution at pH 3.0–8.0 (adjusted using 0.1 M HCl or 0.1 M NaOH) and initial concentration of 5.0–500.0 mg/L was prepared by dilution of stock solutions with distilled water. Then, 10 mg the Fe$_3$O$_4$-NHSO$_3$H@HKUST-1 nanocomposite was added to the solution and the mixture was stirred at various times (5–240 min) and temperatures (15, 25, 35 and 45°C) at a constant speed (150 rpm) by a magnetic stirrer. After the adsorption reached equilibrium, an external magnetic field was applied, which caused the aggregation of the nanocomposite on one side of the beaker. The adsorbed amount of Pb(II) ions was determined as the difference of ion concentration in solution before and after adsorption using AAS. The equilibrium adsorption amount was calculated according to Equation (1):

$$q_e = \frac{(C_0 - C_e)V}{m} \qquad (1)$$

The percent removal (%) of lead ions was calculated using Equation (2):

$$\text{Removal}(\%) = \frac{(C_0 - C_e)}{C_0} \times 100 \qquad (2)$$

In the equations, C_0 and C_e are the initial and the equilibrium concentrations (mg/L) of Pb(II) in solution, respectively, and q_e, V, and m are the quantity of Pb(II) adsorbed on the adsorbent at the time of equilibrium (mg/g), the volume (L) of the solution, and the mass of adsorbent (g) taken for the experiment, respectively.

3 | RESULTS AND DISCUSSION

3.1 | Characterization of the adsorbent

X-ray diffraction (XRD) analysis was used to study the crystal structure of the Fe$_3$O$_4$-NHSO$_3$H@HKUST-1 adsorbent (Figure 2). Figure 2a shows crystalline Fe$_3$O$_4$ (PDF card no. 85-1436), which indicates the crystalline cubic spinel structure of Fe$_3$O$_4$ nanoparticles is maintained during
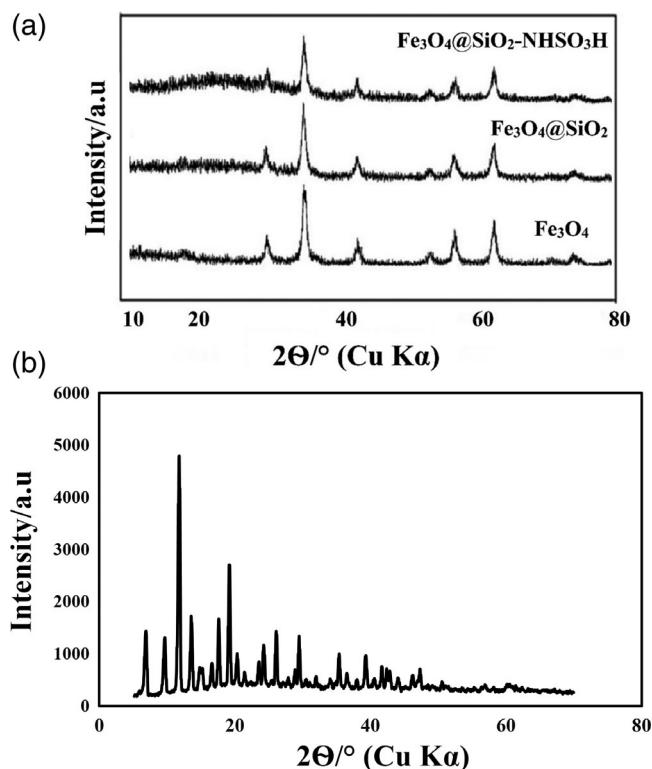
FIGURE 2 XRD pattern of (a) Fe$_3$O$_4$, Fe$_3$O$_4$@SiO$_2$, and Fe$_3$O$_4$@SiO$_2$-NHSO$_3$H nanoparticles and (b) Fe$_3$O$_4$-NHSO$_3$H@HKUST-1 nanocomposite
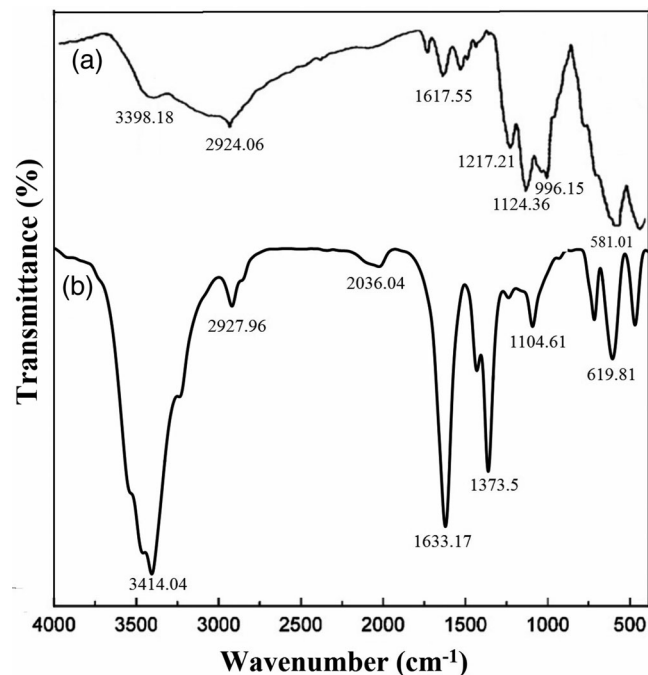
FIGURE 3 FTIR spectra of (a) Fe_3O_4@SiO_2-$NHSO_3H$ and (b) Fe_3O_4-$NHSO_3H$@HKUST-1

FIGURE 5 Nitrogen sorption–desorption isotherms of Fe_3O_4-$NHSO_3H$@HKUST-1

functionalization. Figure 2b shows the decoration of Fe_3O_4-$NHSO_3H$ on HKUST-1, according to the report by Yan Xu et al.,[29] suggesting that the decoration of Fe_3O_4-$NHSO_3H$ on HKUST-1 has not affected the physical characteristics of the MOF, which means the structure of HKUST-1 was well maintained after the modification. The core diameter of the nanocomposite Fe_3O_4-$NHSO_3H$@HKUST-1 was measured to between 20–40 nm, which is more than about 22 nm by using Scherrer's equation ($D = k\lambda/\beta \cos \theta$) from the XRD data.

In Scherrer's equation, k, λ, β, and θ are a constant (0.94), the wavelength of Cu Kα (1.54 A$°$), the corrected diffraction line's full-width at half-maximum, and the Bragg's angle, respectively.
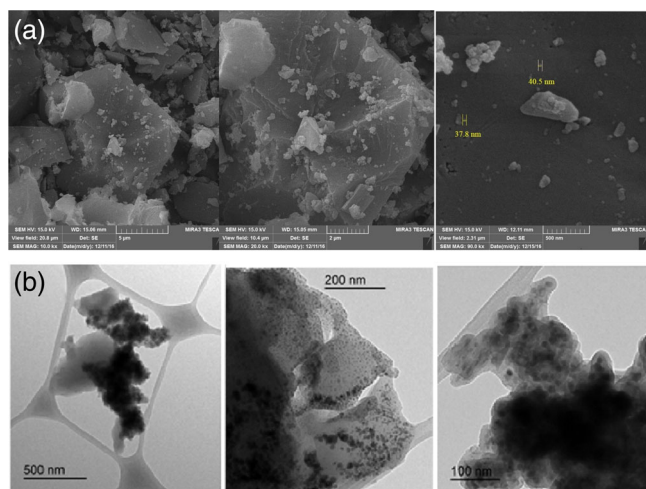
The FTIR spectra of Fe_3O_4@SiO_2-$NHSO_3H$ are displayed in Figure 3a. The Fe–O bands ≤ 700 cm^{-1} indicate the presence of Fe_3O_4.[30] Vibrations belong to Si–OH and Si–H at 996 cm^{-1} indicated to the bonding of TEOS to the MNPs. The peak observed at 3741.6, in turn, was assigned to N–H stretching.[31] The peaks at 1217 and 1124 cm^{-1} are due to the sulfonyl moiety.[28] For Fe_3O_4-$NHSO_3H$@H-KUST-1 (Figure 3b), in addition to the peaks that are related to Fe_3O_4@SiO_2-$NHSO_3H$, the asymmetric stretching vibration at 2927 cm^{-1} was attributed to the aromatic ring C-H in H3BTC, the absorption peaks of the C$=$O bonds (1633 cm^{-1}), and the stretching vibration peaks of C$=$C bonds on the benzene ring (1442 and 1373 cm^{-1})[29] were observed, indicating the formation of Fe_3O_4-$NHSO_3H$@H-KUST-1.

FE-SEM and TEM images were used to describe the morphology and structure of the synthesized Fe_3O_4-$NHSO_3H$@H-KUST-1 nanocomposite (Figure 4). The FE-SEM image (Figure 4a) of as-prepared magnetic nanocomposite clearly shows that the Fe_3O_4-$NHSO_3H$ nanoparticles were located on

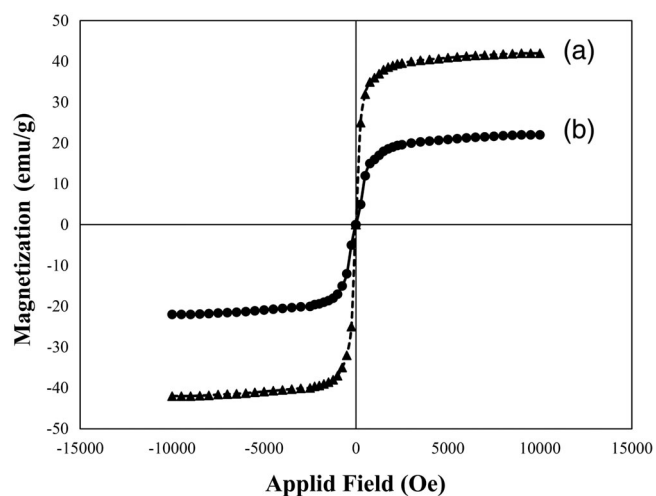**FIGURE 4** (a) FE-SEM and (b) TEM images of the magnetic nanocomposite Fe_3O_4-$NHSO_3H$@HKUST-1

FIGURE 6 VSM measurement of the (a) Fe_3O_4@SiO_2-$NHSO_3H$ and (b) Fe_3O_4-$NHSO_3H$@HKUST-1 nanocomposites

the surface of HKUST-1. However, there are still some bare Fe_3O_4-$NHSO_3H$ nanoparticles not bound to HKUST-1 due to the imperfect reaction. In this study, the size range of the magnetic nanocomposites was about 20–40 nm. The TEM images of the Fe_3O_4-$NHSO_3H$@HKUST-1 nanocomposite were shown in Figure 4b. As can be seen, Fe_3O_4-$NHSO_3H$@H-KUST-1 featuring are a core-shell structure. Furthermore, the TEM images of Fe_3O_4-$NHSO_3H$@HKUST-1 clearly demonstrate that the morphology of Fe_3O_4-$NHSO_3H$ and the particle size of the nanospheres a little with much coarse shell.
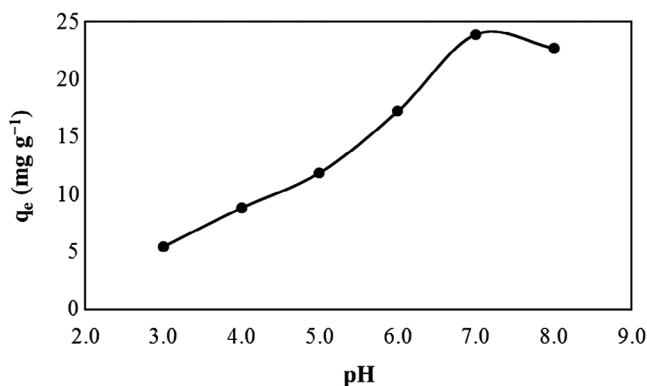
To determine the pore structure parameters of the as-prepared magnetic MOF composites, N_2 adsorption–desorption was also studied (Figure 5). The Brunauer–Emmett–Teller surface area for Fe_3O_4-$NHSO_3H$@HKUST-1 was estimated to be 526 m^2/g with a pore volume 0.590 cm^3/g, which indicates a decrease in the surface of the Fe_3O_4-$NHSO_3H$@HKUST-1 nanocomposite in comparison to the pure HKUST-1 (~1482 m^2/g) due to the coating of the HKUST-1 surface with Fe_3O_4-$NHSO_3H$.[26]

The magnetic properties of Fe_3O_4@SiO_2-$NHSO_3H$ and Fe_3O_4-$NHSO_3H$@HKUST-1 were quantified from −10000 to 10000 Oe (at room temperature) by using VSM magnetometer. As shown in Figure 6, the $M(H)$ hysteresis loops for Fe_3O_4@SiO_2-$NHSO_3H$ and Fe_3O_4-$NHSO_3H$@HKUST-1 were completely reversible, indicating their superparamagnetic behavior. The saturation magnetization value of Fe_3O_4@SiO_2-$NHSO_3H$ nanoparticle is about 42.32 emu/g (Figure 6a), and after decoration of Fe_3O_4@SiO_2-$NHSO_3H$ nanoparticles on the surface of HKUST-1 material, it is 22.16 emu/g (Figure 6b), demonstrating that Fe_3O_4-$NHSO_3H$@HKUST-1 is magnetic.

3.2 | Effective operating parameters

3.2.1 | Effect of pH

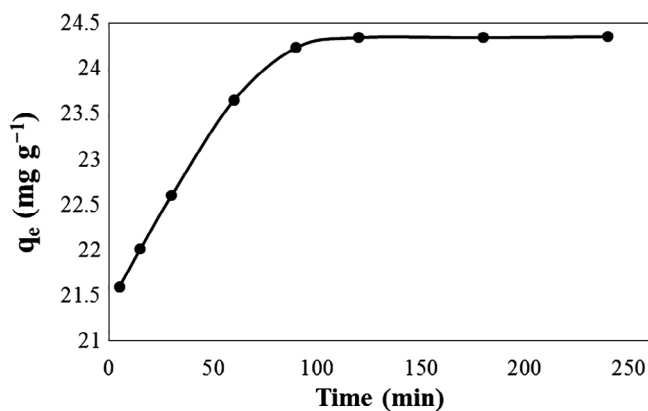The solution pH is one of the factors affecting the adsorption efficiency and reducing the matrix interference in the adsorption process. To verify the effect of solution pH, the adsorption behavior of Pb(II) ions on Fe_3O_4-$NHSO_3H$@H-KUST-1 adsorbent was investigated in pH range of 3.0–8.0 at 25°C by adding 10 mg nanocomposites to 50 mL solution containing 5 mg/L Pb(II) ions and shaking for 240 min (Figure 7). At pH of 3.0–7.0, lead ions co-exist as Pb(II), $Pb(OH)_2$, and $Pb(OH)^+$ ions. There is also Pb(II) ion formation at pH < 3 and as $Pb(OH)_2$ at pH > 7. At acidic pH, the functional groups present on the adsorbent surface easily protonated, and therefore the low adsorption of Pb(II) ions in acidic solution is due to the positive charge of lead ions and adsorbent surface (similar charge).[32] With increase in pH of the solution, the functional groups on the adsorbent surface become deprotonated, which causes increase in the negative charge density on the adsorbent surface, causes the bonding of Pb(II) ions on adsorbent surface. At higher pH, the increase in Pb(II) ions adsorption capacity is also due to the decrease of H^+ ions (Pb(II) ions competitor for adsorption on to the adsorbent active sites).[33] However, with increasing pH, Pb(II) ions get bound to the adsorbent surface, resulting in increased Pb(II) ion adsorption. So, the results indicate that the very excellent adsorption ability of Pb(II) ions on the Fe_3O_4-$NHSO_3H$@HKUST-1 adsorbent is at pH = 7, which could be due to the strong interaction between -SH functional group and lead species.

3.2.2 | Effect of contact time

The time of contact between the adsorbent and adsorbate is one of the main parameters in ion adsorption. The uptake of Pb(II) ions as a function of contact time at pH 7.0, initial concentration of 5.0 mg/L, and temperature 25°C was investigated (Figure 8). Adsorption of Pb(II) ions increased with increase in contact time up to 90 min, but after 90 min the number of Pb(II) ions adsorbed did not change much. The rapid increase in adsorption at the initial stage may be due to the increased accessibility in the number of active binding sites on the adsorbent surface, and the sorption occurs

FIGURE 7 Effect of pH on the adsorption of Pb(II) ions by Fe_3O_4-$NHSO_3H$@HKUST-1 nanoadsorbent (experimental conditions: adsorbent dose 10 mg; agitation speed 150 rpm; contact time 240 min; temperature 298 K; initial concentration 5 mg/L)

FIGURE 8 Effect of contact time on the adsorption of Pb(II) ions by Fe_3O_4-$NHSO_3H$@HKUST-1 adsorbent (experimental conditions: pH 7; adsorbent dose 10 mg; agitation speed 150 rpm, temperature 298 K, initial concentration 5 mg/L)

quickly, which normally controlled by the diffusion process from the bulk to the surface. In the later step, the sorption is likely an attachment-controlled process due to fewer available sorption sites. Therefore, the optimum contact time was considered to be 90 min for lead ion removal under the performed experimental conditions.

### 3.2.3 | Effect of initial Pb(II) concentration

The effect of different initial Pb(II) ion concentrations in the adsorption process by Fe$_3$O$_4$-NHSO$_3$H@HKUST-1 adsorbent is studied. Experiments were carried out by mixing 10 mg of the nanoadsorbent with 50 mL of different initial concentrations of lead ion solutions (5–500 mg/L) at pH 7.0 and contact time of 90 min to investigate the effect of initial lead ion concentration on removal of lead from the solution. The results revealed that there is a strong change in adsorption at low concentrations. Afterwards, a gradual increase was seen in the adsorption with rise concentration up to 300 mg/L, reaching eventually the maximum amount of adsorption. Also the experimental results of this study showed that the large number of active sites of the nanocomposite became saturated approximately at Pb(II) concentration of more than 400 mg/L under the optimum experimental conditions. Hence, the optimum concentration of lead ions to be adsorbed on the Fe$_3$O$_4$-NHSO$_3$H@HKUST-1 nanocomposites was 400 mg/L.

3.2.4 | Effect of solution temperature

To investigate the effect of temperature on the lead ion adsorption on Fe$_3$O$_4$-NHSO$_3$H@HKUST-1, the nanocomposite was tested at four different temperatures (15, 25, 35, and 45°C) by a thermostat attached with a shaker. The results are shown in Figure 9, which clearly indicate that the Pb(II) adsorption increased with temperature rise from 15 to 45°C. This is due to increase in the adsorption capacity with increase in temperature, which causes more mobility and irregularities in molecules during the adsorption process. The higher adsorption capacity at higher temperatures can be
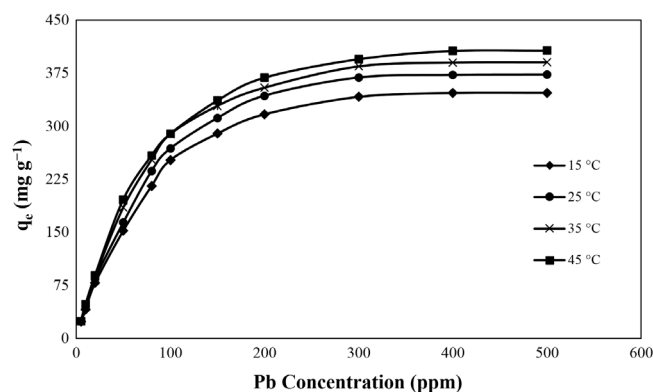
FIGURE 9 Effect of initial Pb(II) concentration and temperature of solution on the adsorption of Pb(II) ions by Fe$_3$O$_4$-NHSO$_3$H@HKUST-1 adsorbent (experimental conditions: pH 7; adsorbent dose 10 mg; agitation speed 150 rpm; contact time 90 min; initial concentration 5 mg/L)
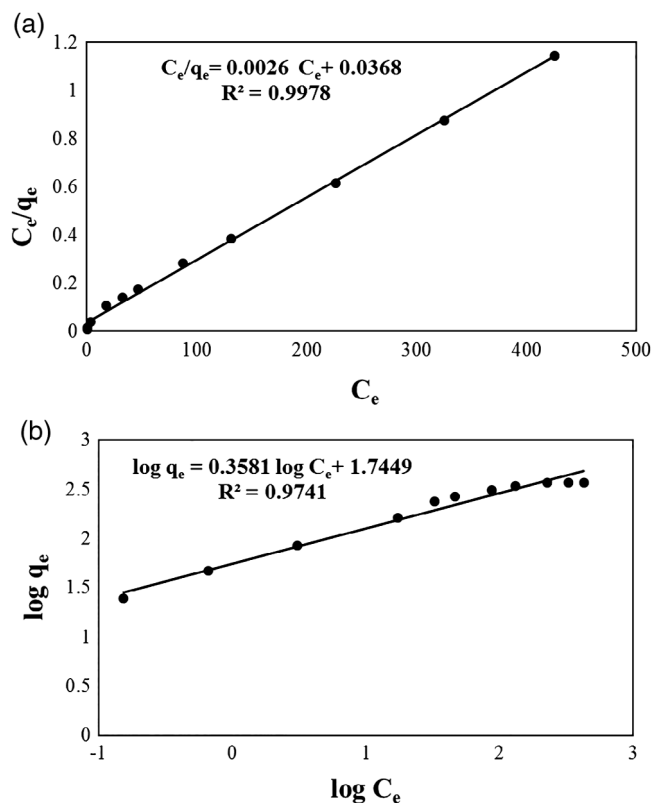
FIGURE 10 Linear plots of (a) Langmuir isotherm and (b) Freundlich isotherm for adsorption of Pb(II) ions by Fe$_3$O$_4$-NHSO$_3$H@HKUST-1 nanoadsorbent (experimental conditions: pH 7; adsorbent dose 10 mg; agitation speed 150 rpm; contact time 90 min; temperature 298 K)

attributed to the expansion of the pore size and increase in activate adsorbent surface area.[34]

3.2.5 | Adsorption isotherms

Adsorption properties and equilibrium parameters, commonly known as adsorption isotherms. Adsorption isotherms give information for the favorable application of nanoadsorbents. The results of adsorption of Pb(II) ions on the Fe$_3$O$_4$-NHSO$_3$H@HKUST-1 adsorbent using Langmuir and Freundlich isotherm models were evaluated. They are expressed as follows[35]:

Langmuir equation:

$$\frac{C_e}{q_e} = \frac{1}{K_L q_m} + \frac{C_e}{q_m} \quad (3)$$

Freundlich equation:

$$\ln q_e = \ln K_F + \frac{1}{n} \ln C_e \quad (4)$$

TABLE 1 Langmuir and Freundlich isotherm parameters for Pb(II) adsorption onto Fe$_3$O$_4$-NHSO$_3$H@HKUST-1

	Langmuir model			Freundlich model		
	q_m (mg/g)	K_L (mg/L)	R^2	K_F	n	R^2
Pb(II)	384.61	0.071	0.998	55.578	2.792	0.974

where q_e (mg/g) and C_e (mg/L) are the amount of metal adsorbed per unit mass of sorbent nanocomposite and the equilibrium concentration of adsorbate in aqueous solution, respectively; q_m (mg/L) and K_L (mg/L) are the maximum value of q_e and the Langmuir equilibrium constant, respectively. K_F (a measure of the adsorption capacity) and n (a measure of the adsorption intensity or surface incongruity) are Freundlich model constants.

Using the slope and intercept of the linear plots of C_e/q_e versus C_e and $\ln q_e$ versus $\ln C_e$ give q_m, K_L and K_F, $1/n$ values, respectively.

The experimental results of Langmuir and Freundlich isotherms are shown in Figure 10. The values of the Langmuir and Freundlich model parameters were calculated using the respective equation and are given in Table 1. The correlation coefficients (R^2) of the Langmuir model was higher for the adsorption of lead ion, indicating that the Langmuir adsorption isotherm more accurately describes the adsorption of Pb(II) on the Fe$_3$O$_4$-NHSO$_3$H@HKUST-1 nanocomposites. According to Langmuir adsorption isotherm, the maximum adsorption capacity for this adsorption process is 384.6 mg/g. Also, the adsorption of Pb(II) ions occurs as a monolayer. Since the specific surface area of the Fe$_3$O$_4$-NHSO$_3$H@HKUST-1 nanocomposites is about 526 m^2/g and the maximum adsorption for Pb(II) onto Fe$_3$O$_4$-NHSO$_3$H@HKUST-1 nanocomposites is 384.6 mg/g, the percentage of occupied sites in this adsorbent is about 46.3%.

3.2.6 | Kinetics of adsorption

To investigate the kinetic mechanism of lead ion adsorption, the adsorption of Pb(II) onto the Fe$_3$O$_4$-NHSO$_3$H@HKUST-1 adsorbent was further studied by adding 10 mg of composites to 50 mL of 5 mg/L Pb(II) solution for different time periods. In this work, two kinetic models were employed as follows[36]:
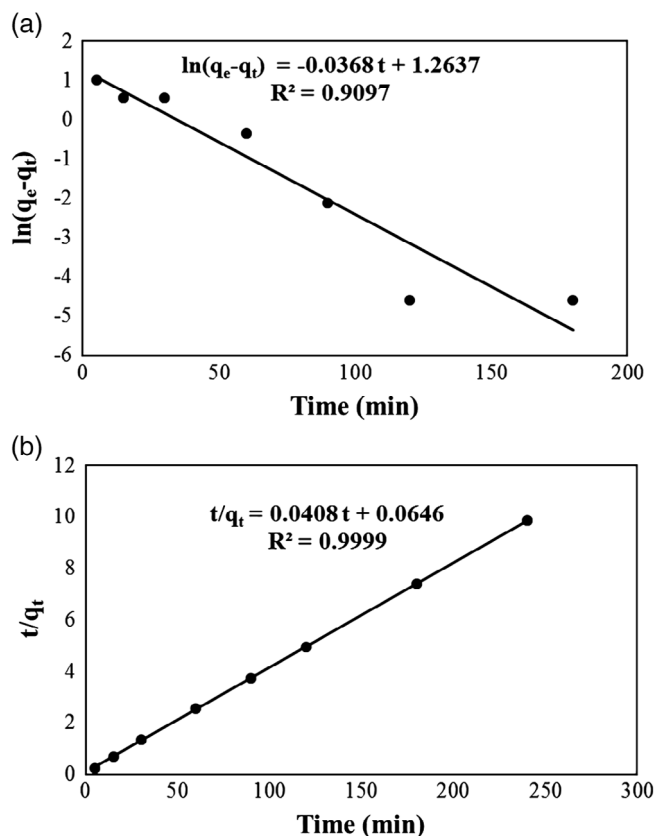
The pseudo-first-order model:

$$\log \left(q_e - q_t \right) = \log q_e - \frac{k_1 t}{2.303} \quad (5)$$

The pseudo-second-order model:

$$\frac{t}{q_t} = \frac{1}{q_e^2 k_2} + \frac{t}{q_e} \quad (6)$$

In the above equations, q_e and q_t (mg/g) are the sorption capacities at equilibrium and at time t, respectively. Also, k_1 (min^{-1}) and k_2 (g mg^{-1} min^{-1}) are the pseudo-first-order rate constant and the pseudo-second-order rate constant, respectively.

The slope and intercept of the linear plot of t/q_t versus t give the values of $1/q_e$ and $1/k_2 q_e^2$, respectively. The experimental results show that 98% lead ions were adsorbed on to the nanocomposites during 10 min, confirming that Fe$_3$O$_4$-NHSO$_3$H@HKUST-1 quickly removes Pb(II) ions from water (Figure 11). Table 2 gives a summary of the models

FIGURE 11 (a) Pseudo-first-order kinetic and (b) pseudo-second-order kinetic plots for the adsorption of Pb(II) on to Fe$_3$O$_4$-NHSO$_3$H@HKUST-1 adsorbent (experimental conditions: pH 7; adsorbent dose 10 mg; agitation speed 150 rpm; contact time 90 min; initial concentration 5 mg/L; temperature 298 K)

TABLE 2 Kinetic parameters for the adsorption of Pb(II) on the Fe$_3$O$_4$NHSO$_3$H@HKUST-1

	Pseudo-first-order kinetic			Pseudo-second-order kinetic		
	k_1 (min^{-1})	q_e (mg/g)	R^2	k_2 (g mg^{-1} min^{-1})	q_e (mg/g)	R^2
Pb(II)	0.039	3.538	0.909	0.026	24.510	0.999

TABLE 3 Thermodynamic parameters for the adsorption of Pb(II) ions on Fe$_3$O$_4$-NHSO$_3$H@HKUST-1 nanoadsorbent

	ΔG^0 (kJ/mol)				ΔS^0 (J K mol^{-1})	ΔH^0 (kJ/mol)
	288(K)	298(K)	308(K)	318(K)	4.842	17.280
Pb(II)	−0.134	−0.307	−0.480	−0.653		

and their corresponding constants along with the correlation coefficients of the linear regression plots of the tested lead ions. As indicated in the table, The correlation coefficient ($R^2 = 0.9999$) of the pseudo-second-order model were obtained more than that of the pseudo-first-order model ($R^2 = 0.9097$), indicating that the adsorption rates of Pb(II) onto the Fe$_3$O$_4$-NHSO$_3$H@HKUST-1 can be properly explained using the pseudo-second-order rate model.

(a)

$$\log K_c = -0.2529 \, 1/T + 0.9025$$
$$R^2 = 0.9843$$

(b)
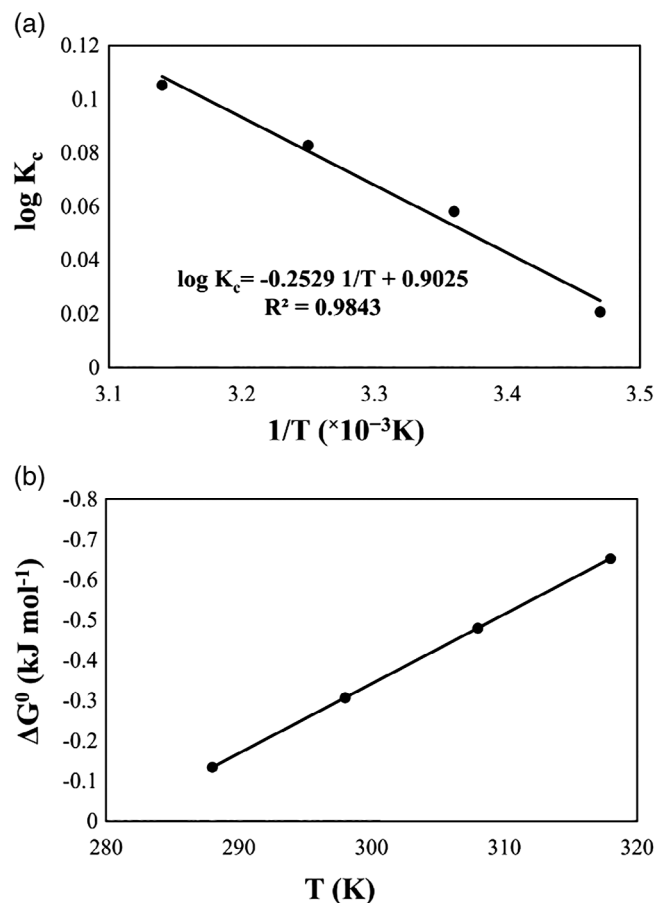
FIGURE 12 Plots of (a) log K_c vs. $1/T$, and (b) $\Delta G°$ vs. T for the adsorbent of Pb(II) ions on the Fe$_3$O$_4$-NHSO$_3$H@HKUST-1 adsorbent (experimental conditions: pH 7; adsorbent dose 10 mg; agitation speed 150 rpm; contact time 90 min; initial concentration 5 mg/L)

3.2.7 | Thermodynamic parameters

The Gibbs free energy change ($\Delta G°$), enthalpy ($\Delta H°$), and entropy ($\Delta S°$) are as thermodynamic parameters that are used to evaluate the thermodynamic behavior of adsorption of Pb(II) on the Fe$_3$O$_4$-NHSO$_3$H@HKUST-1 adsorbent.

The thermodynamic parameters were estimated using the following equations[37,38]:

$$\Delta G^0 = -RT \ln K_c \tag{7}$$

$$\Delta G^0 = \Delta H^0 - T\Delta S^0 \tag{8}$$

where R and K_c are the gas constant and the adsorption equilibrium constant, respectively; the equilibrium constant K_c is the value of q$_e$ versus C$_e$. The free energy change ($\Delta G°$) during the adsorption of Pb(II) onto Fe$_3$O$_4$-NHSO$_3$H@HKUST-1 at four different temperatures was calculated by Equation (8) and are listed in Table 3.

From the slope and intercept of the plot of log K_c versus $1/T$ (Figure 12a), the enthalpy ($\Delta H°$) and entropy ($\Delta S°$) at 288–318 K can be obtained. Their values are also listed in Table 3. The negative amount of free energy change ($\Delta G°$) for the adsorption of Pb(II) onto Fe$_3$O$_4$-NHSO$_3$H@HKUST-1 at the studied range of temperature indicates the

TABLE 4 Comparison of some characteristic data between typical magnetic nanoadsorbents and the proposed magnetic nanoadsorbent for Pb(II) removal

Adsorbent	pH	q_m (mg/g)	Contact time (min)	Temp. (°C)	Ref.
Fe$_3$O$_4$ MNPs/PAA[a]	5	123.3	4320	30	[40]
Fe$_3$O$_4$@SiO$_2$-EDTA[b]	5	114.94	1440	30	[41]
Fe$_3$O$_4$@ silica–xanthan gum	6	21.32	120	20	[42]
Fe$_3$O$_4$@APS@AA-co-CA[c]	5.5	166.1	45	25	[43]
Fe$_3$O$_4$-NHSO$_3$H@HKUST-1	7	384.61	90	25	This work

[a]Multi-functionalized Fe$_3$O$_4$ magnetite nanoparticles/poly(acrylic acid).
[b]EDTA-modified chitosan/SiO$_2$/Fe$_3$O$_4$.
[c]Fe$_3$O$_4$ modified with 3-aminopropyltriethoxysilane and acrylic acid-co-crotonic acid.

spontaneous nature of the adsorption process. The positive value of $\Delta H°$ and $\Delta S°$ for the adsorption of Pb(II) ions represent endothermic and increase of irregularities in the adsorption phenomenon, respectively. Because of the spontaneous and endothermic chemisorption process, the mechanism of Pb(II) ions adsorption is the coordination of Pb^{2+} with –NH$_2$ on surface of Fe$_3$O$_4$-NHSO$_3$H@HKUST-1 adsorbent.[5]

The adsorption system is influenced by the free active sites on the adsorbent and other factors of the adsorption medium such as ion concentration, solution pH, temperature, etc. In this case, because of the coordination mechanism of lead adsorption on the Fe$_3$O$_4$-NHSO$_3$H@HKUST-1 nanocomposite, the combined effects on adsorption of lead ion depend on the solution pH, concentration of coexisting ions, ion–ligand interaction, and ion–ion competition at the active sites of adsorption.[39]

3.2.8 | Sorption and desorption of magnetic MOF Fe$_3$O$_4$-NHSO$_3$H@HKUST-1

Water and HCl (0.1 mol/L) were selected as solvents for the sorption and desorption of Pb(II) ions, respectively.

For the sorption experiment, 10 mg of the Fe$_3$O$_4$-NHSO$_3$H@HKUST-1 nanocomposite was placed in a 100-mL flask, and 50 mL of an aqueous solution of Pb(II) at pH of 7 (5 mg/L) was added to the flask. The mixture was stirred for 90 min at 25°C temperature, then the container containing the mixture was placed near a magnetic field to collect the adsorbent from the solution, and the solution was analyzed.

For the desorption of Pb(II) ions from the adsorbent, the adsorbent (after adsorption) was dispersed in 10 mL of HCl 0.1 M by ultrasonic for 5 min; the adsorbent was finally separated with an external magnet field and washed by distilled water, then dried and reused for the adsorption experiment. The maximum adsorption amount of Pb(II) ions at 90 min and pH of 7 was 98%, indicating that the Pb(II) ions were nearly completely removed from the aqueous solution. The magnetic MOF of Fe$_3$O$_4$-NHSO$_3$H@HKUST-1 could retain

the removal efficiency of Pb(II) ions in > 90% for four cycles.

4 | CONCLUSIONS

This study demonstrated a simple and efficient procedure for the synthesis of a MOF of Fe_3O_4-NHSO$_3$H@HKUST-1 by forming a chemical bond between the Fe_3O_4-NHSO$_3$H nanoparticles and the surface of the MOF for the removal of Pb(II) from aqueous solutions. After determining the structure of the synthesized samples by FTIR, VSM, XRD, and FE-SEM, different factors affecting the removal of lead ions, such as pH of the solution, lead ion concentration, contact time, and temperature, by this nanocomposite were evaluated and optimized. The results indicate that a pseudo-second-order model agrees well with the experimental data. Also the isotherm data were significantly fitted to the Langmuir model. The foundation Fe_3O_4-NHSO$_3$H@HKUST-1 nanocomposite was compared for Pb(II) removal and the distinct features are summarized in Table 4. Because of the different structures and individual properties of MOFs, the Fe_3O_4-NHSO$_3$H@HKUST-1 nanocomposite has high adsorption capacity for the fast and efficient removal of Pb(II) ions from environmental water samples.

ORCID

Mohammad Ali Karimi https://orcid.org/0000-0002-7133-5161

REFERENCES

[1] S. K. Elsaidi, M. H. Mohamed, D. Banerjee, P. K. Thallapally, *Coord. Chem. Rev.* **2018**, *358*, 125.

[2] M. A. Karimi, H. Masrouri, M. A. Mirbagheri, S. Andishgar, T. Pourshamsi, *J. Chin. Chem. Soc.* **2018**, *65*, 1229.

[3] L. Huang, M. He, B. Chen, B. Hu, *Chemosphere* **2018**, *199*, 435.

[4] E. Haque, J. W. Jun, S. H. Jhung, *J. Hazard. Mater.* **2011**, *185*, 507.

[5] Z. Shi, C. Xu, H. Guan, L. Li, L. Fan, Y. Wang, L. Liu, Q. Meng, R. Zhang, *Colloids Surf. A.* **2018**, *539*, 382.

[6] P. A. Kobielska, A. J. Howarth, O. K. Farha, S. Nayak, *Coord. Chem. Rev.* **2018**, *358*, 92.

[7] N. S. Bobbitt, M. L. Mendonca, A. J. Howarth, T. Islamoglu, J. T. Hupp, O. K. Farha, R. Q. Snurr, *Chem. Soc. Rev.* **2017**, *46*, 3357.

[8] N. A. Khan, Z. Hasan, S. H. Jhung, *Adv. Porous Mater.* **2013**, *1*, 91.

[9] J. Ma, G. Wu, S. Li, W. Tan, X. Wang, J. Li, L. Chen, *J. Chromatogr. A* **2018**, *1553*, 57.

[10] X. Zhu, B. Li, J. Yang, Y. Li, W. Zhao, J. Shi, J. Gu, *ACS Appl. Mater. Interfaces* **2014**, *7*, 223.

[11] J. Ma, Z. Yao, L. Hou, W. Lu, Q. Yang, J. Li, L. Chen, *Talanta* **2016**, *161*, 686.

[12] S.-W. Cao, Y.-J. Zhu, M.-Y. Ma, L. Li, L. Zhang, *J. Phys. Chem. C* **2008**, *112*, 1851.

[13] Y. Wang, M. Rui, G. Lu, *J. Sep. Sci.* **2018**, *41*, 180.

[14] F. Tadayon, S. Hosseini, S. Motahar, *J. Chin. Chem. Soc.* **2012**, *59*, 1578.

[15] D. Kavak, *Desalin. Water Treat.* **2013**, *51*, 1720.

[16] A. Mehdinia, D. Jahedi Vaighan, A. Jabbari, *ACS Sustain. Chem. Eng.* **2018**, *6*, 3176.

[17] E. Samper, M. Rodríguez, M. De la Rubia, D. Prats, *Sep. Purif. Technol.* **2009**, *65*, 337.

[18] M. Belkacem, M. Khodir, S. Abdelkrim, *Desalination* **2008**, *228*, 245.

[19] N. P. Hankins, N. Lu, N. Hilal, *Sep. Purif. Technol.* **2006**, *51*, 48.

[20] Q. Li, Y. Xing, Y. Shen, *J. Chin. Chem. Soc.* **2002**, *49*, 535.

[21] E. Ghorbani-Kalhor, *Microchim. Acta* **2016**, *183*, 2639.

[22] X. Cai, J. Li, Z. Zhang, F. Yang, R. Dong, L. Chen, *ACS Appl. Mater. Interfaces* **2013**, *6*, 305.

[23] N. Wang, X.-K. Ouyang, L.-Y. Yang, A. M. Omer, *ACS Sustain. Chem. Eng.* **2017**, *5*, 10447.

[24] M. M. Saeed, S. Z. Bajwa, M. S. Ansari, *J. Chin. Chem. Soc.* **2007**, *54*, 173.

[25] J. Wen, Y. Fang, G. Zeng, *Chemosphere* **2018**, *201*, 627.

[26] F. Ke, L.-G. Qiu, Y.-P. Yuan, F.-M. Peng, X. Jiang, H. Shen, J.-F. Zhu, *J. Hazard. Mater.* **2011**, *196*, 36.

[27] G. Wu, J. Ma, S. Li, J. Guan, B. Jiang, L. Wang, J. Li, X. Wang, L. Chen, *J. Colloid Interface Sci.* **2018**, *528*, 360.

[28] M. Kassaee, H. Masrouri, F. Movahedi, *Appl. Catal. A Gen.* **2011**, *395*, 28.

[29] Y. Xu, J. Jin, X. Li, Y. Han, H. Meng, T. Wang, X. Zhang, *RSC Adv.* **2015**, *5*, 19199.

[30] R. Waldron, *Phys. Rev.* **1955**, *99*, 1727.

[31] M. E. Park, J. H. Chang, *Mater. Sci. Eng. C* **2007**, *27*, 1232.

[32] X. Zhang, S. Lin, X.-Q. Lu, Z.-l. Chen, *Chem. Eng. J.* **2010**, *163*, 243.

[33] M. Taghizadeh, A. A. Asgharinezhad, M. Pooladi, M. Barzin, A. Abbaszadeh, A. Tadjarodi, *Microchim. Acta* **2013**, *180*, 1073.

[34] C. Namasivayam, R. Yamuna, *Chemosphere* **1995**, *30*, 561.

[35] K. Foo, B. Hameed, *Chem. Eng. J.* **2010**, *156*, 2.

[36] S. Laurent, D. Forge, M. Port, A. Roch, C. Robic, L. Vander Elst, R. N. Muller, *Chem. Rev.* **2008**, *108*, 2064.

[37] S. Chowdhury, R. Mishra, P. Saha, P. Kushwaha, *Desalination* **2011**, *265*, 159.

[38] S. Chowdhury, P. Saha, *Chem. Eng. J.* **2010**, *164*, 168.

[39] A. L. Taka, E. Fosso-Kankeu, K. Pillay, X. Y. Mbianda, *Environ. Sci. Pollut. Res.* **2018**, *25*, 21752.

[40] L. Jiang, F. Chai, Q. Chen, *Eur. Polym. J.* **2017**, *89*, 468.

[41] Y. Liu, R. Fu, Y. Sun, X. Zhou, S. A. Baig, X. Xu, *Appl. Surf. Sci.* **2016**, *369*, 267.

[42] X. Peng, F. Xu, W. Zhang, J. Wang, C. Zeng, M. Niu, E. Chmielewská, *Colloids Surf A Physicochem. Eng. Asp.* **2014**, *443*, 27.

[43] F. Ge, M.-M. Li, H. Ye, B.-X. Zhao, *J. Hazard. Mater.* **2012**, *211*, 366.